Optics Letters

Fractal superconducting nanowire single-photon detectors with reduced polarization sensitivity

Xiaoming Chi,[1,2] Kai Zou,[1,2] Chao Gu,[1,2] Julien Zichi,[3] Yuhao Cheng,[1,2] Nan Hu,[1,2] Xiaojian Lan,[1,2] Shufan Chen,[1,2] Zuzeng Lin,[1,2,3] Val Zwiller,[3] and Xiaolong Hu[1,2,*]

[1]School of Precision Instrument and Optoelectronic Engineering, Tianjin University, Tianjin 300072, China
[2]Key Laboratory of Optoelectronic Information Science and Technology, Ministry of Education, Tianjin 300072, China
[3]Department of Applied Physics, Royal Institute of Technology (KTH), SE-106 91 Stockholm, Sweden
*Corresponding author: xiaolonghu@tju.edu.cn

Received 6 August 2018; revised 15 September 2018; accepted 16 September 2018; posted 17 September 2018 (Doc. ID 341593); published 9 October 2018

We demonstrate superconducting nanowire single-photon detectors (SNSPDs) based on a fractal design of the nanowires to reduce the polarization sensitivity of detection efficiency. We patterned niobium titanium nitride thin films into Peano curves with a linewidth of 100 nm and integrated the nanowires with optical microcavities to enhance their optical absorption. At a base temperature of 2.6 K, the fractal SNSPD exhibited a polarization-maximum device efficiency of 67% and a polarization-minimum device efficiency of 61% at a wavelength of 1550 nm. Therefore, the polarization sensitivity, defined as their ratio, was 1.1, lower than the polarization sensitivity of the SNSPDs in the meander design. The reduced polarization sensitivity of the detector could be maintained for higher-order spatial modes in multimode optical fibers and could tolerate misalignment between the optical mode and the detector. This fractal design is applicable to both amorphous and polycrystalline materials that are commonly used for making SNSPDs.

OCIS codes: (030.5260) Photon counting; (270.0270) Quantum optics; (230.0040) Detectors.

https://doi.org/10.1364/OL.43.005017

The detection efficiency of superconducting nanowire (nanostripe) single-photon detectors [1] (SNSPDs, also referred to as SSPDs) in meander designs are sensitive to the polarization states of the incident photons [2–6]. For example, if the incident photons are from the HE_{11} spatial mode of an optical fiber, the detection efficiency for the HE_{11y} mode, with the electric field oscillating along the nanowire, is higher than that for the HE_{11x} mode, with the electric field oscillating orthogonal to the nanowire. The cause of this polarization sensitivity of the detection efficiency [2,7] is that the distribution along the x direction (the width direction of the nanowire) of the local optical absorptance [8], $a(x)$, of a straight, y-direction-oriented nanowire in a meander design is polarization-dependent. This effect, similar to the effect used in a metal wire grid polarizer, makes (1) the overall optical absorptance [8], $A = \int_{-w/2}^{w/2} a(x)\mathrm{d}x/w$, where w is the width of the nanowire, and (2) the overall internal quantum efficiency [8], $P = \int_{-w/2}^{w/2} p(x)a(x)\mathrm{d}x/\int_{-w/2}^{w/2} a(x)\mathrm{d}x$, where $p(x)$ is the local internal quantum efficiency [8], both polarization-dependent. Consequently, the overall device efficiency (DE) [8], $\mathrm{DE} = \int_{-w/2}^{w/2} p(x)a(x)\mathrm{d}x/w$, is also polarization-dependent.

To reduce the polarization sensitivity of SNSPDs, several approaches have been demonstrated: (1) patterning the nanowire into spiral structures [4,6], (2) side-by-side making two orthogonally oriented meanders that are electrically connected in series [4], and (3) making double-layer, two orthogonally oriented meanders that are electrically connected in parallel [5]. These approaches successfully reduced the polarization sensitivity of the SNSPDs.

In this Letter, we demonstrate the reduction of the polarization sensitivity of SNSPDs using the fractal design of the nanowires that were proposed in Ref. [9] and discuss its additional advantages compared with the approaches that have been previously demonstrated. In a broader context, we note that the concepts of fractal structures have been used for making mechanically stretchable interconnects to conduct DC current [10] and antennas to transmit and receive microwave signals [11]. Our work was directly inspired by the former. However, to the best of our knowledge, applying the fractal concept to boosting the performance of single-photon detectors in the infrared spectral range has never been reported.

We used Peano curves [9] as examples to illustrate the concept of the fractal SNSPDs and to realize our proof-of-principle devices. We note that other types of fractal curves, such as Hilbert and Moore curves [10,12], should work equally well. The intuition for proposing this design [9] was that these fractal curves would eliminate the orientation of the nanowire on the global view of a device, and therefore, P, A, and DE would become polarization-independent. Figure 1 presents the scanning electron micrographs of the nanowires in the Peano structure that we patterned on a niobium titanium nitride (NbTiN) thin film. Specifically, the geometry of the nanowire in Fig. 1(a)

is a first-order Peano curve. To expand the area covered by the nanowire, nine first-order Peano nanowires are connected in series to form a second-order Peano nanowire, as shown in Fig. 1(b). We similarly continued this process to obtain the third-order one, expanding the covering area by a factor of 9, as shown in Fig. 1(c). We then connected four third-order Peano nanowires in series to form a detector covering a 9.1 μm × 9.1 μm active area, as shown in Fig. 1(d), that was used in our experiment. The red dashed lines in (b) and (c) show the self-similarity among different orders of the fractal nanowire. The width of the nanowire is 100 nm; the fill factor, defined as the area that the nanowire directly covers over the total active area, is 59%.

We integrated the nanowire with an optical cavity to enhance its optical absorption [13,14]. Figure 2(a) shows a schematic drawing of the device structure, and Fig. 2(b) shows the plane-view optical micrograph of a device that we fabricated. The substrate was a double-sided thermally oxidized silicon wafer with a 280-nm-thick silicon oxide layer. The NbTiN thickness was 9 nm. The top spacer was evaporated silicon oxide with thickness optimized using Comsol Multiphysics to maximize optical absorption of the nanowire at 1550 nm. The optical refractive indices of silicon oxide, silicon, NbTiN, and gold, used in our simulation at a wavelength of 1550 nm, are 1.44, 3.63, $4.563 + i4.911$ [15], and $0.52 + i10.74$ [16], respectively. Figure 2(c) shows the simulated optical absorption of the nanowire in a fractal design. According to our simulation, the optimum thickness of the top spacer, L_c, is 210 nm for both HE_{11x} and HE_{11y} modes for SNSPDs in the fractal design. The optimal optical absorption is 96% for both HE_{11x} and HE_{11y} modes. In comparison, Fig. 2(d) shows the simulated optical absorption for the meander design with a 100 nm nanowire width and a 200 nm pitch (i.e., 50% fill factor). For the SNSPD in the meander design with the same spacer thickness, 210 nm, the optical absorptance for HE_{11x} and HE_{11y} modes is 75% and 86%, respectively.

We briefly present the device fabrication process. A 9-nm-thick NbTiN film was deposited for 82 s by reactive magnetron cosputtering from two ultrapure targets of Ti and Nb in an Ar/N_2 gas mixture at room temperature. The nanowires were patterned using scanning electron beam lithography with an accelerating voltage of 100 kV. The resist was a 150-nm-thick layer of polymethylmethacrylate (PMMA, 950k). Both the fractal and the meander structures were patterned on the same

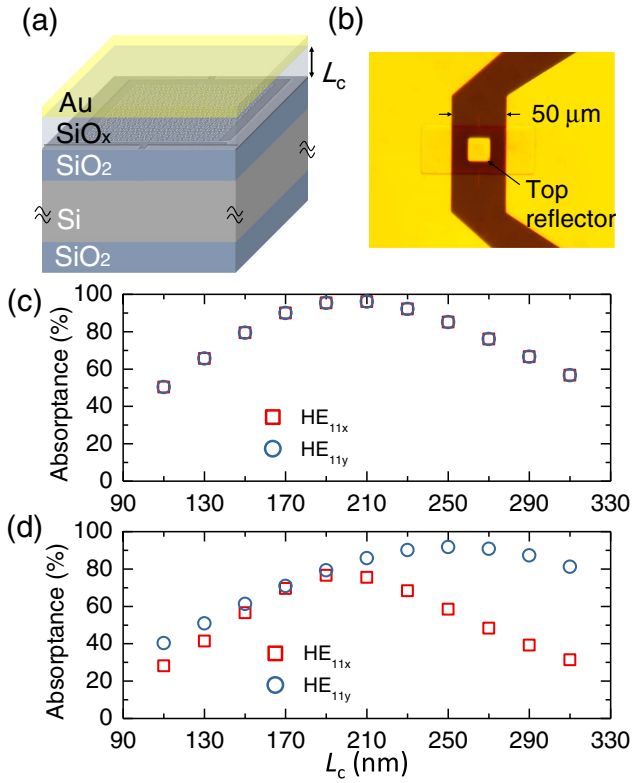

Fig. 2. Enhancement of optical absorption using a microcavity. (a) A schematic drawing of the device structure. (b) An optical micrograph of the fabricated superconducting nanowire single-photon detector. (c) Simulated optical absorptance of the nanowires in the fractal design (100 nm wide, 59% fill factor) for photons from the HE_{11x} and HE_{11y} modes. (d) Simulated optical absorptance of the nanowires in the meander design (100 nm wide, 50% fill factor) for photons from the HE_{11x} and HE_{11y} modes.

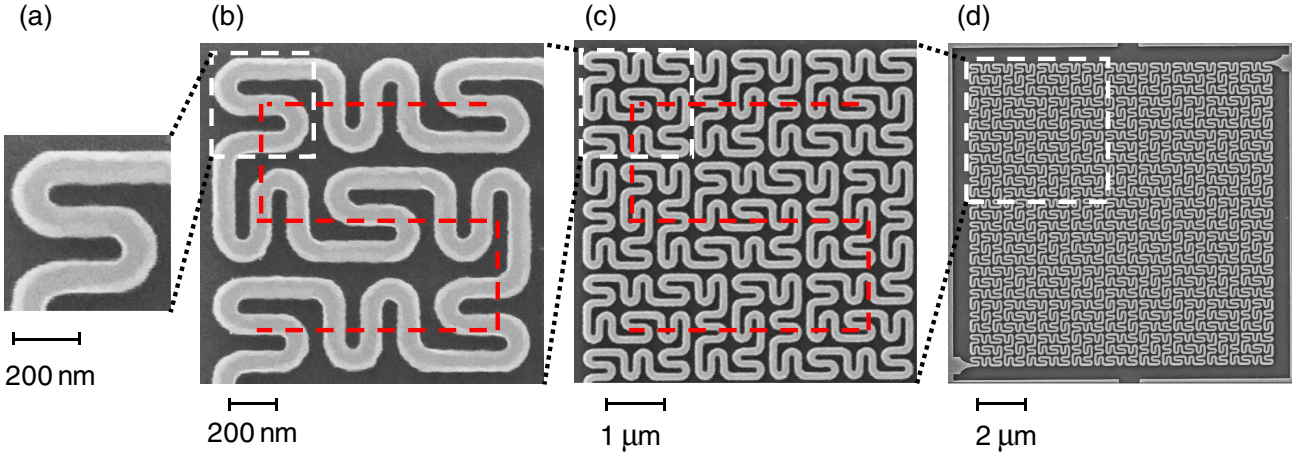

Fig. 1. Scanning electron micrographs of a superconducting nanowire single-photon detector (SNSPD) in the fractal design. (a), (b), and (c) are the nanowires in the shape of the first-, second-, and third-order Peano curves, respectively. (d) is the structure that connects four third-order Peano nanowires in series and forms the active area of the SNSPD. The red dashed lines in (b) and (c) show the self-similarity among different orders of the fractal nanowire.

chip to make a comparison of their performance. After developing the resist in a 1:3 mixture of methyl isobutyl ketone and isopropanol for 40 s, the pattern was transferred onto the NbTiN film by reactive-ion etching with CF_4 (15 sccm, 100 W RF power, at a pressure of 2.7 Pa) for 30 s. We removed the remaining resist by soaking the chip in N-Methyl pyrrolidone (NMP) at 90°C for 5 h. We then defined the aligned electrical contact pads with optical lithography using NR9-3000PY photoresist. After developing the resist, 5 nm Ti and 100 nm Au were evaporated. The lift-off process was done by soaking the chip in NMP at 90°C for 30 min. The top spacer made of silicon oxide and the top reflector made of Ti/Au were added by similar optical lithography, e-beam evaporation, and lift-off steps. Finally, we etched away the remaining nonpatterned NbTiN using the top spacer as a mask to make proper electrical connections of the detectors.

We tested the SNSPDs in a closed-cycle cryocooler, with cooling power of 1 W at the cold head. The chip was mounted on a homemade chip holder, and the chip holder was attached to the cold head of the cryocooler. A base temperature of 2.6 K was measured with a temperature sensor mounted adjacent to the chip. The optical source used was a pigtailed continuous wave semiconductor laser at a wavelength of 1550 nm. A polarization controller and an in-line polarimeter module were used to control and measure the polarization state of the incident light, respectively. The light was attenuated by an adjustable precision optical attenuator. The standard single-mode optical fiber entered the cryocooler through a FC/PC fiber vacuum feedthrough. To measure the DE, we used a broad illumination scheme: a fiber focuser, customized from Ozoptics, was installed on the chip holder and illuminated the detector from the back side through the substrate. The working distance, from the top facet of the fiber focuser to the top surface of the chip, was 28.5 mm. The spot size, defined as the diameter where the light intensity drops to $1/e^2$ of the maximum intensity of the Gaussian beam, at this working distance was 15.8 mm. We calculated the coupling efficiency by taking into account the location of the device under test relative to the center of the incident beam. A low-noise voltage source and low-noise 100-kΩ resistor were used to bias the SNSPD. Two RF amplifiers with 58 dB gain in total amplified the pulses, which were then sent into either an oscilloscope for inspecting the waveforms or a universal counter to count the electrical pulses.

To characterize the polarization sensitivity of the SNSPDs, we first searched the polarization-maximum DE, $\mathrm{DE}(\alpha)_{\max}$; the corresponding polarization state, $\alpha_{\max}$; the polarization-minimum DE, $\mathrm{DE}(\alpha)_{\min}$; and the corresponding polarization state, $\alpha_{\min}$, by scanning the polarization state, α, over the Poincaré sphere, keeping the bias current to be $I_b = 0.95I_{sw}$, where I_{sw} is the switching current of the SNSPD; then $\mathrm{DE}(\alpha)_{\max}$ and $\mathrm{DE}(\alpha)_{\min}$ were measured as a function of the bias current, and $\mathrm{DE}(\alpha)$, at different polarization states on the largest circle going through $\alpha_{\max}$ and $\alpha_{\min}$ on the Poincaré sphere, was measured. Figure 3 presents the measured DE and its polarization dependence of the fractal SNSPD and the meander SNSPD that were made on a same chip.

The measured I_{sw} of the fractal SNSPD is 7.5 μA, lower than that of the meander SNSPD, which is 10.5 μA, due to the current-crowding effect at the turns [17,18]. We simulated the sheet current density, $K(x, y)$, close to the turns of the Peano nanowire and the turns of the meander using Comsol Multiphysics based on finite element method. The sheet current density, K, obeys [17] $\nabla \cdot K = 0$ and $\nabla \times K = 0$. The simulation shows that if these two nanowires, in the fractal design and in the meander design, are biased with the same I_b, then the ratio between the maximum sheet current density in the meander design and the maximum sheet current density in the fractal design equals to 0.718. This result means that the ratio of the switching current between the fractal SNSPD and the meander SNSPD is 0.718, comparable to the experimental value, 0.714. The current-crowding effect and the resulting reduction of the switching current make the DE not saturated, even at the I_b approaching I_{sw}, for the fractal SNSPD, as presented in Fig. 3(a).

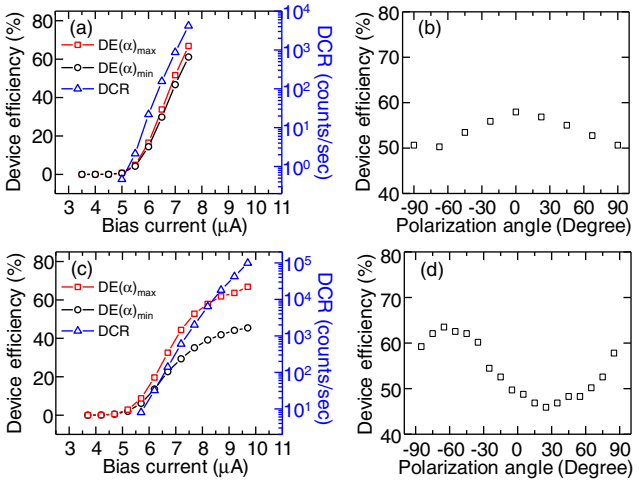

Fig. 3. Device efficiency (DE) and its polarization dependence. (a) The polarization-maximum DE, $\mathrm{DE}(\alpha)_{\max}$, the polarization-minimum DE, $\mathrm{DE}(\alpha)_{\min}$, and the dark-count rates (DCRs) of the fractal superconducting nanowire single-photon detector (SNSPD), as a function of bias current; (b) the polarization-dependent DE of the fractal SNSPD at the bias current $I_b = 0.95I_{sw}$ ($I_{sw} = 7.5$ μA); (c) $\mathrm{DE}(\alpha)_{\max}$, $\mathrm{DE}(\alpha)_{\min}$, and DCRs of the meander SNSPD, as a function of bias current; (d) the polarization-dependent DE of the meander SNSPD at the bias current $I_b = 0.95I_{sw}$ ($I_{sw} = 10.5$ μA).

Figure 3 shows that the polarization sensitivity of the fractal SNSPD is lower than that of the meander SNSPD. Figure 3(b) presents the polarization-dependent DE of the fractal SNSPD at the bias current $I_b = 0.95I_{sw}$, and the polarization sensitivity was calculated to be 1.15. In comparison, Fig. 3(d) presents the polarization-dependent DE of the meander SNSPD at the bias current $I_b = 0.95I_{sw}$, and the polarization sensitivity was calculated to be 1.38. When the fractal SNSPD was fully biased, $\mathrm{DE}(\alpha)_{\max} = 67\%$, $\mathrm{DE}(\alpha)_{\min} = 61\%$, and the maximum dark-count rate (DCR) was ~4200 counts/sec. In comparison, the DE of the meander SNSPD, as presented in Fig. 3(c), more slowly increases when I_b approaches I_{sw}. When this meander SNSPD was fully biased, $\mathrm{DE}(\alpha)_{\max} = 67\%$, $\mathrm{DE}(\alpha)_{\min} = 46\%$, and the maximum DCR was ~99000 counts/sec. We note that as shown in Fig. 2(d), the thickness of the top spacer, 210 nm, is not the value that maximizes the optical absorption and therefore, $\mathrm{DE}(\alpha)_{\max}$, for the meander SNSPD. If the meander SNSPD was made with the spacer thickness that would maximize $\mathrm{DE}(\alpha)_{\min}$ as typical meander SNSPDs were designed, its resulting

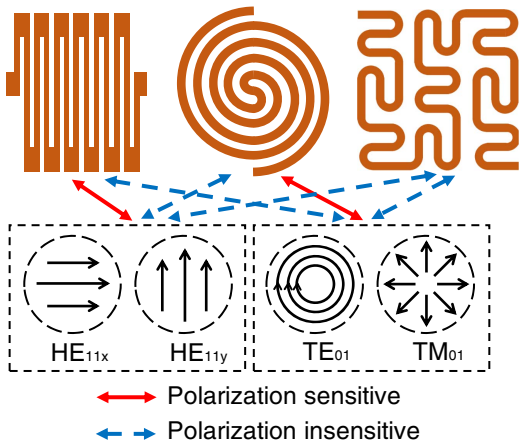

Fig. 4. Schematic drawing of a meander design, a spiral design, and a fractal design of superconducting nanowire single-photon detectors and the expected polarization dependence of their responses to the photons in the HE_{11x}, HE_{11y}, TE_{01}, and TM_{01} modes.

polarization sensitivity would be larger. We also note that the measured maximum DCR of the fractal SNSPD is significantly lower than that of the meander one, although the fractal one contains more U-turns in its pattern. However, whether the fractal SNSPDs—when with the similar maximum device efficiencies as their meander counterparts—would generally show lower maximum DCRs and, therefore, higher signal-to-noise ratios, remains open and needs more experimental and theoretical investigations.

In the context of polarization-insensitive SNSPDs, a major advantage of the fractal SNSPD is that the reduced polarization sensitivity can be maintained for high-order spatial modes of multimode optical fibers, for example, TE_{01} and TM_{01} modes. In comparison, the spiral SNSPDs [4,6] become polarization-sensitive for these modes. We schematically illustrate this comparison in Fig. 4. This hypothesis was supported by our preliminary three-dimensional (3D) simulations on the optical absorptance of the nanowires in the meander, spiral, and fractal SNSPDs when the incident photons are in the HE_{11x}, HE_{11y}, TE_{01}, and TM_{01} modes and the comparison of the polarization sensitivity of the optical absorptance. As space-division multiplexing technology [19] in classical optical communications uses higher-order modes of optical fibers as the additional information channels to expand the capacity, we argue that making the SNSPDs polarization-insensitive for photons from these higher-order modes would be useful for future photon-counting applications that use these modes. Additionally, the fractal SNSPDs do not require accurate alignment between the optical spatial mode and the active area in order to obtain low polarization sensitivity. In contrast, the polarization sensitivity of the orthogonally oriented, side-by-side meanders [4] depends on the alignment. These two advantages are due to the fact that the fractal designs locally (i.e., in the second- and third-order fractal structures) eliminate the orientation of the nanowires rather than globally average out the orientations as the two-orthogonal meanders and the spirals did. Finally, compared with 3D WSi detectors [5], the one layer nature of the fractal SNSPDs makes the fabrication process simpler. Of course, this fractal design is applicable to both amorphous and polycrystalline superconducting materials for making SNSPDs.

In summary, we have demonstrated a fractal SNSPD with a DE over 60% at a wavelength of 1550 nm and a reduced polarization sensitivity of 1.1. We have also presented the advantages of fractal device structure in the context of polarization-insensitive SNSPDs. We believe that the fractal SNSPDs would be useful in applications where polarization-independent single-photon detection is needed.

Funding. National Natural Science Foundation of China (NSFC) (61505141, 11527808); Natural Science Foundation of Tianjin Municipal Science and Technology Commission (15JCYBJC52500).

Acknowledgment. We would like to thank Professors Kaiyu Cui at Tsinghua University, Yidong Huang at Tsinghua University, and Guifang Li at Tianjin University for use of their equipment; Dr. Weijie Sun at Beijing Institute of Nanoenergy and Nanosystems, Chinese Academy of Sciences for technical assistance in scanning electron beam lithography; and Ms. Lanqin Yan and Mr. Xiaojun Li at National Center for Nanoscience and Technology for technical assistance in e-beam evaporation and reactive-ion etching, respectively.

REFERENCES

1. G. N. Gol'tsman, O. Okunev, G. Chulkova, A. Lipatov, A. Semenov, K. Smirnov, B. Voronov, A. Dzardanov, C. Williams, and R. Sobolewski, Appl. Phys. Lett. **79**, 705 (2001).
2. V. Anant, A. J. Kerman, E. A. Dauler, J. K. Yang, K. M. Rosfjord, and K. K. Berggren, Opt. Express **16**, 10750 (2008).
3. E. F. C. Driessen, F. R. Braakman, E. M. Reiger, S. N. Dorenbos, V. Zwiller, and M. J. A. de Dood, Eur. Phys. J. **47**, 10701 (2009).
4. S. N. Dorenbos, E. M. Reiger, N. Akopian, U. Perinetti, V. Zwiller, T. Zijlstra, and T. M. Klapwijk, Appl. Phys. Lett. **93**, 161102 (2008).
5. V. B. Verma, F. Marsili, S. Harrington, A. E. Lita, R. P. Mirin, and S. W. Nam, Appl. Phys. Lett. **101**, 251114 (2012).
6. J. Huang, W. J. Zhang, L. X. You, X. Y. Liu, Q. Guo, Y. Wang, L. Zhang, X. Y. Yang, H. Li, Z. Wang, and X. M. Xie, Supercond. Sci. Technol. **30**, 074004 (2017).
7. J. J. Renema, R. Gaudio, Q. Wang, Z. Zhou, A. Gaggero, F. Mattioli, and M. P. V. Exter, Phys. Rev. Lett. **112**, 117604 (2014).
8. H. Wu, C. Gu, Y. Cheng, and X. Hu, Appl. Phys. Lett. **111**, 062603 (2017).
9. C. Gu, Y. Cheng, X. Zhu, and X. Hu, in *Novel Optical Materials and Applications* (Optical Society of America, 2015), paper JM3A.10.
10. J. A. Fan, W. Yeo, Y. Su, Y. Hattori, W. Lee, S. Y. Jung, Y. Zhang, Z. Liu, H. Cheng, L. Falgout, M. Bajema, T. Coleman, D. Gregoire, R. J. Larsen, Y. Huang, and J. A. Rogers, Nat. Commun. **5**, 3266 (2014).
11. D. H. Werner, R. L. Haupt, and P. L. Werner, IEEE Antennas Propag. Mag. **41**(5), 37 (1999).
12. H. Sagan, *Space-Filling Curves* (Springer, 2012).
13. K. M. Rosfjord, J. K. Yang, E. A. Dauler, A. J. Kerman, V. Anant, B. M. Voronov, G. N. Gol'tsman, and K. K. Berggren, Opt. Express **14**, 527 (2006).
14. X. Hu, T. Zhong, J. E. White, E. A. Dauler, F. Najafi, C. H. Herder, F. N. Wong, and K. K. Berggren, Opt. Lett. **34**, 3607 (2009).
15. S. Miki, T. Yamashita, H. Terai, and Z. Wang, Opt. Express **21**, 10208 (2013).
16. P. B. Johnson and R. W. Christy, Phys. Rev. B **6**, 4370 (1972).
17. J. R. Clem and K. K. Berggren, Phys. Rev. B **84**, 174510 (2011).
18. H. L. Hortensius, E. F. C. Driessen, T. M. Klapwijk, K. K. Berggren, and J. R. Clem, Appl. Phys. Lett. **100**, 182602 (2012).
19. G. Li, N. Bai, N. Zhao, and C. Xia, Adv. Opt. Photon. **6**, 413 (2014).